JOURNAL OF THERMOPHYSICS AND HEAT TRANSFER
Vol. 10, No. 4, October–December 1996

Simple Harmonic Analysis of Regenerators

G. W. Swift* and W. C. Ward†
Los Alamos National Laboratory, Los Alamos, New Mexico 87545

A simple harmonic analysis of the performance of regenerators is described. Computer calculations based on the simple harmonic analysis run orders of magnitude faster than time-integration methods, with acceptably small reductions in accuracy. This simple harmonic analysis method is based on previous one-dimensional differential equations of heat and mass flow, with the additional assumption of steady-state operation and with the key approximations that only the magnitudes and phases of the fundamental components of time-dependent variables are of interest and that the instantaneous friction-factor and heat transfer coefficients are determined from the instantaneous velocity via steady-flow correlations. This permits a rapid computation scheme in which complex amplitudes of oscillatory variables are used, without numerical time integrations. The method is presented here using the Kays and London correlations for stacked-screen regenerators, but it can be used for any regenerator matrix for which steady friction-factor and heat transfer correlations exist.

I. Introduction

THE hydrodynamics and thermodynamics of oscillatory flow through solid matrices are of great interest to researchers studying Stirling machines because the highest efficiencies are achieved only with the most carefully engineered regenerators. This is especially true for Stirling cryocoolers, for which even slight regenerator ineffectiveness can cause significant decreases in net cooling power.

Although such oscillatory flow is theoretically well understood in simple geometries such as arrays of circular tubes, many Stirling regenerators comprise stacked screens and other complex geometries, for which computational methods are still evolving and fundamental data are sadly lacking. Organ[1] points out many of the shortcomings of the current state of the art. However, given today's imperfect foundations, we may justifiably make additional approximations if they improve computational ease dramatically, while only slightly reducing accuracy.

Regenerator computation methods may be grouped into three classes: 1) time stepped, 2) globally implicit, and 3) perturbation. All of these methods use one-dimensional equations of hydrodynamics and thermodynamics, with variables representing spatial averages over volumes large enough to smooth over the details of each individual screen. Organ[1] has reviewed several examples of these methods.

In the time-stepped methods[2] the regenerator is spatially discretized into a large number of segments and the governing differential equations are converted to finite difference equations for the segments. With appropriate boundary conditions, the finite difference equations are then processed for sequential time steps much shorter than the thermodynamic cycle period until a periodic steady state is reached, typically after many thermodynamic cycle periods, and hence, exceedingly many computation time steps. In contrast to the other two classes, time-stepped methods provide transient as well as steady-state results, but they unfortunately require the greatest computation time.

The globally implicit class[3] handles spatial dependence in the same way as the time-step methods, but discretizes time over a single period of the thermodynamic cycle only, imposing time-periodic boundary conditions on all variables. By thus computing the periodic steady-state results directly, the globally implicit method requires less computation time than steady-state methods.

Finally, the perturbation computation methods use the fact that selected variables are small for all cases of interest. For example, Bauwens'[4] nearly isothermal analysis assumes that the oscillatory components of temperature are small compared to the mean temperatures. Further simplification can be achieved by assuming that all oscillating variables are small and have simple-harmonic time dependence. The work presented here is in this class. Important antecedents include a linearized Stirling machine analysis as reviewed by Urieli and Berchowitz[5] (with no effort at detailed regenerator analysis), the wave analysis of Organ[6] (with the temperature profile along the regenerator taken as given), the thermoacoustic approach of Xiao,[7,8] and the linear network analysis of Huang and Lu.[9,10] In an important advance for harmonic methods, Xiao used the constancy of a time-averaged energy flux along the regenerator to self-consistently compute the regenerator temperature profile; however, he did not use amplitude-dependent friction-factor and heat transfer coefficients. Huang and Lu gave closed-form solutions for pressure and mass flux, in a very clear network–analysis formalism using experimentally based amplitude-dependent friction-factor and heat transfer coefficients. However, they did not discuss energy flux and, in particular, they did not use constancy of time-averaged energy flux to self-consistently compute the regenerator temperature profile; instead, they simply assigned a single effective average temperature to the entire regenerator when computing its dynamic response. For the extreme temperature gradients often found in modern cryocoolers, this approximation is inadequate.

Our new simple harmonic analysis method combines the simplicity and computational speed of Xiao's method with the use of amplitude-dependent friction factor and heat transfer coefficient data. We follow most of the physical approximations of the time-step method of Gary et al.,[2] including the assumption that the friction factor and heat transfer coefficient at each instant of time are determined by the instantaneous velocity via measured steady-state correlations. However, our method uses the additional key assumptions that all time-dependent variables are simple harmonic and that the regenerator is in steady state. We believe that this is the first complete, correct use of amplitude-dependent friction factor and heat transfer in a harmonic analysis.

With these assumptions, we compute with only the spatially-dependent amplitudes and phases of time-dependent variables,

Received May 11, 1995; revision received Nov. 30, 1995; accepted for publication April 20, 1996.

*Staff Member, Condensed Matter and Thermal Physics Group.
†Staff Member, Energy Process Engineering Group.

so that computations can be extremely fast (orders of magnitude faster than time-stepped methods). We sacrifice accuracy by imposing linear approximations on the nonlinear equations of hydrodynamics and thermodynamics. For pressure oscillations of order 20% of mean pressure, and/or oscillatory velocities of order 20% of the sound speed, we can expect errors of order 20% because of the harmonic approximation. A few additional simplifying approximations are made whenever we expect them to contribute errors no larger than this.

In this report, we base our computations on the stacked screen friction factor and heat transfer data of Kays and London,[11] to facilitate comparison of our results to those of Gary et al.,[2] who also use the Kays and London correlations. Our method, however, is fundamentally independent of the Kays and London correlations. It allows the incorporation of any steady-state friction-factor and heat transfer correlations, for stacked screens or for any other complex regenerator geometry,[12] into a harmonic analysis in a self-consistent manner that uses the full amplitude-dependent information in the correlations.

We now clearly establish the notation to be used. We will consider a stacked screen regenerator of length L and cross-sectional area A. The porosity ϕ is the ratio of gas volume to total regenerator volume, so that ϕAL is the total volume of gas in the regenerator. The hydraulic radius r_h of the regenerator is the ratio of total gas volume to the gas–solid interface surface area (commonly referred to as wetted area). (For circular pores, the hydraulic radius is half the circle radius.) Expressions for the hydraulic radius of stacked-screen regenerators as a function of porosity and wire diameter are presented by Organ.[1]

We will assume that an expansion to first order in the oscillatory amplitude suffices for any dynamic variable ξ, so that it can be written

$$\xi(\boldsymbol{r}, t) \simeq \xi_m(\boldsymbol{r}) + \mathrm{Re}[\xi_1(\boldsymbol{r})e^{i\omega t}] \tag{1}$$

where $\boldsymbol{r}$ is the vector position, t is time, ω is the angular frequency of the oscillation, and Re[ ] signifies the real part. The mean value (subscript m) of ξ is a real number, but the small amplitude of the time–oscillatory part (subscript 1) is a complex number, reflecting time phasing of the oscillating quantity. In keeping with the usual convention, we will often omit Re[ ] when no confusion is likely to arise. For time-averaged products of variables $\overline{\xi(t)\psi(t)}$ in expressions for average power (where the overbar denotes the time average), we will use

$$\overline{\xi(t)\psi(t)} = \xi_m\psi_m + \mathrm{Re}[\xi_1\tilde{\psi}_1]/2 \tag{2}$$

where the tilde denotes complex conjugation.

Equation (1) is the key approximation for simple harmonic methods. The steady-state assumption is equivalent to the fact that $\xi_m(\boldsymbol{r})$ is independent of time. The only time dependence is $e^{i\omega t}$, showing our neglect of all higher-order Fourier components.

In some of the discussion to follow, it will be necessary to distinguish carefully between the value of a variable at a point in space and its spatially averaged value over a small region. Figure 1a shows a microscopic view of a portion of a stacked-screen regenerator. At some typical point A in the regenerator, the instantaneous velocity v_1 is unlikely to be along the direction of acoustic oscillation (the x direction), and may be relatively large or small depending on the distance of point A from the nearest solid surface. For most of our discussion, we will be interested only in the local spatial average velocity, averaged over a region such as the dashed area shown in Fig. 1b, where distances are large compared to the screen wire size, but small enough that spatially averaged quantities do not vary appreciably over the region. In the case of velocity, such an average value will be in the x direction; we denote it as $\langle u_1\rangle$. Mean variables do not have microscopic spatial dependence,

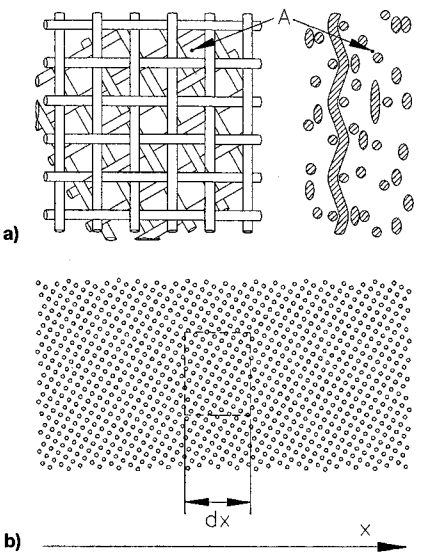

Fig. 1 Two views of stacked screen regenerator: a) microscopic view, both plan and cross section, in which the values of variables such as velocity vary wildly from point A to nearby points, and b) the locally averaged view, in which local-average variables are smoothly varying.

nor does the pressure amplitude, but for velocity, temperature, and density amplitudes we will at first distinguish between their microscopic values v_1, T_1, and ρ_1 and their local spatial averages $\langle u_1\rangle$, $\langle T_1\rangle$, and $\langle \rho_1\rangle$. We adopt the convention that these averages are taken over the volume of gas enclosed in the dashed region of Fig. 1b. The dependences of these variables are summarized in Table 1. We will often omit explicitly writing the dependences when there is no ambiguity, as with $\langle u_1\rangle$, which depends only on x according to Table 1.

We will regard p_1, $\langle u_1\rangle$, and T_m as the dependent variables of interest. Given their values at one end, we will derive a procedure for numerically generating $p_1(x)$, $\langle u_1(x)\rangle$, and $T_m(x)$ throughout the regenerator, using equations of the form

$$\frac{dp_1}{dx} = F_1(p_1, \langle u_1\rangle, T_m, \bar{H}_2, \text{geometry}) \tag{3}$$

$$\frac{d\langle u_1\rangle}{dx} = F_2(p_1, \langle u_1\rangle, T_m, \bar{H}_2, \text{geometry}) \tag{4}$$

$$\frac{dT_m}{dx} = F_3(p_1, \langle u_1\rangle, T_m, \bar{H}_2, \text{geometry}) \tag{5}$$

Equation (3) will be derived largely from friction factor data. Equation (4) will be derived from the continuity equation, and Eq. (5) from the equation for time-averaged energy flux $\bar{H}_2$ through the regenerator; both of the latter will use heat transfer coefficient data. Equations of this form permit numerical integration beginning at one end of the regenerator at which values of all variables are known.

We have imbedded this computation scheme in an iterative algorithm[13] so that mixed boundary conditions can be accommodated. Typically, T_m and $\langle u_1\rangle$ might be known at both ends of the regenerator; the algorithm then uses $\bar{H}_2$ and p_1 at the starting end of the regenerator as guessed initial conditions, adjusting them until the targeted values of T_m and $\langle u_1\rangle$ are reached at the other end.

Because p_1 and $\langle u_1\rangle$ are complex, Eqs. (3–5) actually represent five real first-order differential equations. A minor, fundamental shortcoming of the simple harmonic method and of all previous methods arises from the fact that two data sets (friction factor and heat transfer) are insufficient to generate these five equations. We will see that the friction factor data

Table 1 Summary of dependences of important variables

Variables	General, microscopic	Harmonic, microscopic	Harmonic, local spatial average
Velocity	$v(r, t)$	$=v_1(r)e^{i\omega t}$	$\rightarrow\langle u_1(x)\rangle e^{i\omega t}$
Temperature	$T(r, t)$	$=T_m(x) + T_1(r)e^{i\omega t}$	$\rightarrow T_m(x) + \langle T_1(x)\rangle e^{i\omega t}$
Pressure	$p(r, t)$	$=p_m(x) + p_1(x)e^{i\omega t}$	$\rightarrow$Same
Density	$\rho(r, t)$	$=\rho_m(x) + \rho_1(r)e^{i\omega t}$	$\rightarrow\rho_m(x) + \langle\rho_1(x)\rangle e^{i\omega t}$

provide a solid foundation for the dissipative component of the dp_1/dx equation, and the heat transfer data provide a solid foundation for the dT_m/dx equation. Rough approximations suffice for the inertial component of the dp_1/dx equation and for the reversible component of the $d\langle u_1\rangle/dx$ equation, because they do not contribute directly to energy flux or mechanical power. But accurate development of the irreversible part of the $d\langle u_1\rangle/dx$ equation, which does contribute to mechanical power dissipation, requires a new set of fundamental data. Like previous methods, the simple harmonic method will, for the present, get by as well as possible without such data.

II. Derivation Details

A. Momentum Equation: dp_1/dx

We begin with the simplest of the three gradients we must compute, dp_1/dx, which we obtain from the momentum (or Navier–Stokes) equation. Following the method given by Xiao[7] and by Huang and Lu,[9] but with a slightly different notation, we write the one-dimensional momentum equation in the harmonic approximation as

$$\frac{dp_1}{dx} = -i\omega\rho_{\text{eff}}\langle u_1\rangle - \Phi\langle u_1\rangle \tag{6}$$

where ρ_{eff} is the effective mean mass density that accounts for the tortuosity of the flow path through the screens and Φ accounts for the effects of viscosity. Terms such as $i\omega\rho_1 u_1$ and $\rho_m u_1 \partial u_1/\partial x$, present in the Navier–Stokes equation, are neglected in Eq. (6) because they are second order in the small oscillatory amplitudes.

The two terms on the right-hand side (RHS) of Eq. (6) are the inertial and dissipative contributions to the pressure gradient. We begin with the dissipative term. To obtain Φ we realize that in screens and other complex Stirling regenerators the gas displacement amplitude is much larger than r_h and, hence, the frequency with which the velocity of a given microscopic piece of gas varies in time[1] is of the order of $\langle u_1\rangle/r_h$, which is much higher than ω. Under these circumstances, we can assume that the instantaneous pressure gradient is related to the instantaneous velocity in the same way that pressure gradient is related to velocity in steady, unidirectional flow. In other words, we can assume that the steady-state friction factor is directly applicable at each instant of time, independent of the past history of the flow. This assumption, shared by time-step analyses of regenerators,[2] implies that

$$\frac{\partial p(x, t)}{\partial x} = -\frac{1}{2}\rho(t)|\langle u(t)\rangle|\langle u(t)\rangle\frac{f(t)}{r_h} \tag{7}$$

where f is the friction factor, usually tabulated as a function of Reynolds number

$$Re = 4|\langle u\rangle|r_h\rho/\mu \tag{8}$$

and porosity.

To make further progress, we must pick a specific functional form for $f(Re)$. For screens, we chose to use the data plotted in Fig. 7.9 of Kays and London.[11] (Our principal motivation for choosing these data is to facilitate comparison of our results to the time-step method of Gary et al.,[2] which uses the same data.) In the figure, as $Re \rightarrow 0$, $f \propto 1/Re$, as must be the case to ensure that $dp/dx \propto \langle u\rangle$. It is therefore plausible to fit f with

$$f \simeq c_1(\phi)/Re + c_2(\phi) \tag{9}$$

Appendix A includes our particular choices for the functions $c_n(\phi)$ and comparisons of the resulting Eq. (9) to the data of Kays and London.

In the simple harmonic approximation, our goal is to derive an expression for the fundamental Fourier component of Eq. (7). Using Eqs. (8) and (9) to write $f(t)$ more explicitly, we find that Eq. (7) becomes

$$\frac{\partial p(x, t)}{\partial x} = -\frac{\mu(t)}{r_h^2}\langle u(t)\rangle\left[\frac{c_1(\phi)}{8} + \frac{c_2(\phi)r_h|\langle u(t)\rangle|\rho(t)}{2\mu(t)}\right] \tag{10}$$

For our purposes, we can express μ and ρ by first-order Taylor series expansions:

$$\mu(t) = \mu_m + \left(\frac{\partial\mu}{\partial T}\right)[T(t) - T_m] + \left(\frac{\partial\mu}{\partial p}\right)[p(t) - p_m] \tag{11}$$

and similarly for ρ. We use these expansions in Eq. (10), substitute expressions of the form of Eq. (1) for $\langle u(t)\rangle$, $p(t)$, and $T(t)$, multiply the entire equation by $e^{-i\omega t}/\pi$, and integrate the resulting expression with respect to ωt from 0 to 2π.

On the left-hand side (LHS) of Eq. (10), this procedure produces simply dp_1/dx, the desired result. On the RHS, the first of the two terms reduces easily to $[\mu_m c_1(\phi)/8r_h^2]\langle u_1\rangle$. In the second term, we neglect T_1 and p_1 because their contributions are third or fourth order in the small oscillatory amplitudes. With this approximation, and putting Eq. (10) in the form of Eq. (6), we obtain finally

$$\frac{dp_1}{dx} = -i\omega\rho_{\text{eff}}\langle u_1\rangle - \frac{\mu_m}{r_h^2}\left[\frac{c_1(\phi)}{8} + \frac{c_2(\phi)Re_1}{3\pi}\right]\langle u_1\rangle \tag{12}$$

where

$$Re_1 = 4|\langle u_1\rangle|r_h\rho_m/\mu_m \tag{13}$$

(Re_1 is a positive real number, not a complex number.)

This result depends, of course, on our specific choice of Kays and London[11] data for $f(Re)$. However, the method, deriving the complex fundamental Fourier component of dp_1/dx from steady-state friction factor data, is general enough to use for any $f(Re)$, for screens or any other complex regenerator geometry.

Equation (12) can be regarded as defining an effective friction factor $f_{\text{eff}} = c_1(\phi)/Re_1 + 8c_2(\phi)/3\pi$ as a function of peak Reynolds number Re_1, which gives the dependence of the amplitude of oscillatory pressure drop on the amplitude of oscillatory velocity through the screens. Tanaka et al.[14] measured $4f_{\text{eff}} \simeq 175/Re_1 + 1.6$ in four screen regenerators with porosities ϕ ranging from 0.645 to 0.754. Our values of $c_n(\phi)$ given in Appendix A yield $4f_{\text{eff}} = 160/Re_1 + 1.7$ and $4f_{\text{eff}} \simeq 165/Re_1 + 1.2$ at $\phi = 0.645$ and 0.754, respectively, in good agreement with the experiments. Hence, this part of our results is essentially identical to that of Huang and Lu,[10] who use the data of Tanaka et al. directly.

The inertial term is much smaller than the dissipative term in typical regenerators. It has no direct influence on effectiveness, and so it is generally neglected in regenerator analyses; for our purposes, a rough, inviscid approximation will suffice. We know that ρ_m is lower bound on ρ_{eff}, because the flow passages in the regenerator cannot be less tortured than straight, parallel-sided passages. A plausible upper bound on ρ_{eff} can be obtained by considering a regenerator geometry comprising alternating, equal-length open and constricted sections in series, with straight, parallel-sided passages in all sections, and with porosity 1 in the open sections and porosity $2\phi - 1$ in the constricted sections. It is straightforward to show for this case that $\rho_{\text{eff}} = \rho_m\phi^2/(2\phi - 1)$. We simply use the average of the upper and lower bounds as our estimate of ρ_{eff}:

$$\rho_{\text{eff}} = \rho_m[1 + (1 - \phi)^2/2(2\phi - 1)] \tag{14}$$

For a typical value of $\phi \simeq 0.65$, Eq. (14) differs from either of the bounds on ρ_{eff} by 20%. For typical regenerators we have considered the inertial term in Eq. (12) is at most 1% of the dissipative term, and so this uncertainty in ρ_{eff} is quite acceptable. However, for extremely high-frequency, extremely tortured passages, or for porosity below 0.6, a more accurate expression for ρ_{eff} would be needed.

Equation (12), with Eq. (14) for ρ_{eff}, is the first of the three equations we seek; it is of the form of Eq. (3).

B. Oscillatory Temperature

To obtain an expression for the complex amplitude of the oscillatory temperature in the gas, we will first derive a differential equation for the velocity-weighted average gas temperature, and then impose the harmonic condition on its solution as we did for Eq. (10).

We begin by considering the heat transfer coefficient h, usually defined as the ratio of heat flux per unit wetted area to temperature difference from one side of the wetted area to the other, with the gas-side temperature a heat-capacity-flux-density weighted average[11] rather than a simple spatial average. Hence, we should write

$$\frac{\text{heat flux}}{\text{wetted area}} = \left(T_s - \frac{\langle \rho c_p u T\rangle}{\langle \rho c_p u\rangle}\right) h \tag{15}$$

where T_s is the solid's temperature. We will make the important assumption that h depends only on the instantaneous value of the Reynolds number, not on the past history of the flow, for the same reasons that we made this assumption for f earlier.

Now consider the general equation of heat transfer

$$\rho c_p \frac{\partial T}{\partial t} - T\beta \frac{\partial p}{\partial t} + \rho c_p \boldsymbol{v}\cdot\nabla T - T\beta \boldsymbol{v}\cdot\nabla p = \nabla\cdot(K\nabla T) \tag{16}$$

(where K is thermal conductivity), from the microscopic point of view embodied in Fig. 1a. This equation holds exactly in the microscopic view in the gas-filled space. Next, we perform a local spatial average of Eq. (16) over the gas volume in a portion of the regenerator of length dx and cross-sectional area A. This integration does not include the volume occupied by the screen wires; hence, the total volume over which the integration is performed is $\phi A\ \mathrm{d}x$. On the RHS, we use Green's theorem to express the volume integral of the divergence of the heat flux density $K\nabla T$ as a surface integral over the gas–solid wetted area S within the volume of integration. The result is

$$\phi A\ \mathrm{d}x \left(\left\langle \rho c_p \frac{\partial T}{\partial t}\right\rangle - \langle T\beta\rangle \frac{\partial p}{\partial t} + \langle \rho c_p \boldsymbol{v}\cdot\nabla T\rangle - \langle T\beta \boldsymbol{v}\cdot\nabla p\rangle\right) = \int \mathrm{d}S\ K\nabla T \tag{17}$$

Using the definition of h, we obtain finally

$$\left\langle \rho c_p \frac{\partial T}{\partial t}\right\rangle - \langle T\beta\rangle \frac{\partial p}{\partial t} + \langle \rho c_p \boldsymbol{v}\cdot\nabla T\rangle - \langle T\beta \boldsymbol{v}\cdot\nabla p\rangle = -\frac{h(Re)}{r_h}\left(\frac{\langle \rho c_p u T\rangle}{\langle \rho c_p u\rangle} - T_s\right) \tag{18}$$

A similar, but simpler, derivation yields an analogous equation for the solid temperature, which is assumed spatially uniform on the microscopic length scale:

$$\rho_s c_s \frac{1-\phi}{\phi}\frac{\partial T_s}{\partial t} = \frac{h(Re)}{r_h}\left(\frac{\langle \rho c_p u T\rangle}{\langle \rho c_p u\rangle} - T_s\right) \tag{19}$$

We can simplify Eqs. (18) and (19) if we anticipate our later use of the form of Eq. (1) for all variables except h and neglect terms of order higher than one now. The result is

$$\rho_m c_{p,m}\frac{\partial\langle T\rangle}{\partial t} - T_m\beta_m\frac{\partial p}{\partial t} + \rho_m c_{p,m}\langle u\rangle\frac{\mathrm{d}T_m}{\mathrm{d}x} = -\frac{h(Re)}{r_h}\left(\frac{\langle uT\rangle}{\langle u\rangle} - T_s\right) \tag{20}$$

$$\rho_{s,m}c_{s,m}\frac{1-\phi}{\phi}\frac{\partial T_s}{\partial t} = \frac{h(Re)}{r_h}\left(\frac{\langle uT\rangle}{\langle u\rangle} - T_s\right) \tag{21}$$

Eliminating T_s from Eqs. (20) and (21) yields

$$\frac{\partial}{\partial t}\left(\frac{\langle uT\rangle}{\langle u\rangle}\right) + \varepsilon_s\frac{\partial\langle T\rangle}{\partial t} + \rho_m c_{p,m} r_h \frac{\partial}{\partial t}\left[\frac{1}{h(Re)}\frac{\partial\langle T\rangle}{\partial t}\right] = \varepsilon_s\left(\frac{T_m\beta_m}{\rho_m c_{p,m}}\frac{\partial p}{\partial t} - \langle u\rangle\frac{\mathrm{d}T_m}{\mathrm{d}x}\right) + \rho_m c_{p,m} r_h \frac{\partial}{\partial t} \times \left[\frac{1}{h(Re)}\left(\frac{T_m\beta_m}{\rho_m c_{p,m}}\frac{\partial p}{\partial t} - \langle u\rangle\frac{\mathrm{d}T_m}{\mathrm{d}x}\right)\right] \tag{22}$$

where

$$\varepsilon_s = \phi\rho_m c_{p,m}/(1-\phi)\rho_{s,m}c_{s,m} \tag{23}$$

gives the ratio of gas heat capacity to solid heat capacity.

Typically, regenerators have $\varepsilon_s \ll 1$ and large h. Examination of Eq. (22) shows that $\partial\langle T\rangle/\partial t$ is then small (of order ε_s or $1/h$), and so the second and third terms on the LHS are of second order in the small quantities. In those two small terms, we ignore the distinction between the local spatial average temperature $\langle T\rangle$ and its velocity-weighted average

$$\langle T\rangle_u \equiv \langle uT\rangle/\langle u\rangle \tag{24}$$

We then rewrite Eq. (22) as

$$(1+\varepsilon_s)\frac{\partial\langle T\rangle_u}{\partial t} + \rho_m c_{p,m} r_h \frac{\partial}{\partial t}\left[\frac{1}{h(Re)}\frac{\partial\langle T\rangle_u}{\partial t}\right] = \varepsilon_s\left(\frac{T_m\beta_m}{\rho_m c_{p,m}}\frac{\partial p}{\partial t} - \langle u\rangle\frac{\mathrm{d}T_m}{\mathrm{d}x}\right) + \rho_m c_{p,m} r_h \frac{\partial}{\partial t} \times \left[\frac{1}{h(Re)}\left(\frac{T_m\beta_m}{\rho_m c_{p,m}}\frac{\partial p}{\partial t} - \langle u\rangle\frac{\mathrm{d}T_m}{\mathrm{d}x}\right)\right] \tag{25}$$

The plausibility of Eq. (25) is apparent in two simple limits. First, if $h \to \infty$, the solid and gas have the same temperature $\langle T\rangle_u$ at each instant of time. In this case, Eq. (25) reduces to

$$[\phi\rho_m c_{p,m} + (1-\phi)\rho_{s,m}c_{s,m}]\frac{\partial\langle T\rangle_u}{\partial t} = \phi\left(T_m\beta_m\frac{\partial p}{\partial t} - \rho_m c_{p,m}\langle u\rangle\frac{dT_m}{dx}\right) \quad (26)$$

showing how the temperature responds to the rate of heat generation per unit volume. The quantity in brackets on the LHS is the total heat capacity per unit volume of regenerator. The quantity in parentheses on the RHS is the rate of heat generation (from pressure changes and from gas flow) per unit volume of gas; multiplying by ϕ gives the rate of heat generation per unit volume of regenerator.

Second, if instead $\varepsilon_s = 0$ (i.e., the solid's heat capacity is large) and h is independent of Re, Eq. (25) can be integrated with respect to time to yield

$$\langle T\rangle_u - T_s = \frac{r_h}{h}\left(T_m\beta_m\frac{\partial p}{\partial t} - \rho_m c_{p,m}\langle u\rangle\frac{dT_m}{dx} - \rho_m c_{p,m}\frac{\partial\langle T\rangle_u}{\partial t}\right) \quad (27)$$

showing that the heat generated per unit volume of gas is partly absorbed by the specific heat of the gas, with the balance flowing across h with temperature difference $\langle T\rangle_u - T_s$.

To make further progress, we must pick a specific functional form for h. As described in Appendix A, we write h for stacked screens in the form

$$h(Re) = \frac{b(\phi)\sigma^{1/3}}{4}\frac{K}{r_h}(1 + Re^{3/5}) \quad (28)$$

where σ is the Prandtl number of the gas, and use Fig. 7-8 of Kays and London[11] to obtain $b(\phi)$. (Our principal motivation for choosing these data is to facilitate comparison to a time-step method[2] that uses the same data.)

To solve Eq. (25) for $\langle T\rangle_u$ in the simple harmonic approximation, we use the form of Eq. (1) for each of $\langle T\rangle_u$, $\langle u\rangle$, and p, with Eq. (28) for h and Eq. (8) for Re. We then multiply the entire equation by $e^{-i\omega t}/\pi$ and integrate from 0 to 2π with respect to ωt to select the complex fundamental Fourier component of the equation. The details of this calculation, which depend on our choice of Eq. (28) for $h(Re)$, are outlined in Appendix C. The result is

$$\langle T\rangle_{u,1} = \frac{T_m\beta_m}{\rho_m c_{p,m}}\frac{\varepsilon_s + (g_c + e^{2i\theta_p}g_v)\varepsilon_h}{1 + \varepsilon_s + (g_c + e^{2i\theta_T}g_v)\varepsilon_h}p_1 - \frac{1}{i\omega}\frac{dT_m}{dx}\frac{\varepsilon_s + (g_c - g_v)\varepsilon_h}{1 + \varepsilon_s + (g_c + e^{2i\theta_T}g_v)\varepsilon_h}\langle u_1\rangle \quad (29)$$

where

$$g_c(Re_1) = \frac{2}{\pi}\int_0^{\pi/2}\frac{dz}{1 + Re_1^{3/5}\cos^{3/5}(z)} \quad (30)$$

$$g_v(Re_1) = -\frac{2}{\pi}\int_0^{\pi/2}\frac{\cos(2z)\,dz}{1 + Re_1^{3/5}\cos^{3/5}(z)} \quad (31)$$

$$\varepsilon_h = 8ir_h^2/b(\phi)\sigma^{1/3}\delta_\kappa^2 \quad (32)$$

$$\delta_\kappa^2 = 2K_m/\omega\rho_m c_{p,m} \quad (33)$$

$$\theta_p = \text{phase}(\langle u_1\rangle) - \text{phase}(p_1) \quad (34)$$

$$\theta_T = \text{phase}(\langle u_1\rangle) - \text{phase}(\langle T\rangle_{u,1}) \quad (35)$$

Plots of g_c and g_v, which depend on our specific choice of Eq. (28) for $h(Re)$, are shown in Appendix B.

Examination of Eq. (29) shows it to be quite plausible. The oscillations in temperature are caused by two sources: 1) pressure and 2) velocity. Without the screens, the oscillating pressure would cause an adiabatic oscillating temperature $T_m\beta_m p_1/\rho_m c_{p,m}$, and the oscillating velocity would cause an oscillating temperature $(dT_m/dx)\langle u_1\rangle/i\omega$ proportional to (and in phase with) the oscillating displacement amplitude $\langle u_1\rangle/i\omega$. With the screens, if $h \to \infty$, the temperature oscillations are reduced by the factor

$$\frac{\varepsilon_s}{1 + \varepsilon_s} = \frac{\phi\rho_m c_{p,m}}{\phi\rho_m c_{p,m} + (1-\phi)\rho_{s,m}c_{s,m}} \quad (36)$$

to account for the ratio of gas heat capacity to total heat capacity. Finally, with h finite instead of infinite, $\langle T\rangle_{u,1}$ is increased by an amount depending on the degree of thermal contact, roughly proportional to $g_c r_h^2/\delta_\kappa^2$. At high Reynolds number, this decreases with Reynolds number, reflecting the improved thermal contact caused by vigorous flow; in the low Reynolds number limit, the increase in $\langle T\rangle_{u,1}$ reduces to the square of the ratio of the hydraulic radius to the thermal penetration depth δ_κ. Note that, for most regenerators, the factor $1 + \varepsilon_s + (g_c + e^{2i\theta_T}g_v)\varepsilon_h$ in the denominators of Eq. (29) is approximately 1, equivalent to our comments previous to Eq. (24) regarding small terms in which the distinction between $\langle T_1\rangle$ and $\langle T\rangle_{u,1}$ can be neglected.

We will discuss the interpretation of Eq. (29) in terms of an effective cycle-averaged heat transfer coefficient for oscillatory flow in Sec. II.D.

C. Energy Equation: dT_m/dx

We obtain an equation for dT_m/dx from consideration of the total energy flux along the regenerator, which must be independent of x because the side boundaries of the regenerator are well insulated. The energy flux density is $\rho v(v^2/2 + w) - K\nabla T - v\cdot\Sigma$, where w is the enthalpy per unit mass. We will neglect the term with the viscous stress tensor Σ and the v^3 kinetic energy term because they are third order in the small oscillatory quantities, so that the energy flux density reduces to $\rho vw - K\nabla T$. By averaging over time, taking the local spatial integral over area A and length dx as shown in Fig. 1b, and inserting expressions of the form of Eq. (1), we find the total time-averaged energy flux $\bar{H}_2$ to second order:

$$\bar{H}_2 \simeq \phi A\rho_m\overline{\text{Re}[u_1e^{i\omega t}]\text{Re}[w_1e^{i\omega t}]} - (1-\phi)AK_{\text{eff}}\frac{dT_m}{dx} \quad (37)$$

Here, K_{eff} is an effective local average longitudinal thermal conductivity that takes into account the sporadic nature of the metal-to-metal contact between adjacent screens in the stack. The contribution of the gas to the local average longitudinal thermal conductivity is negligible in comparison to that of the screens. Gary et al.[2] suggest that $K_{\text{eff}} \simeq 0.3K_{s,m}$ for typical metal screens. Equation (37) does not contain a term $\overline{\langle\rho v\rangle}w_m$ because the time-averaged, spatial-average mass flow $\overline{\langle\rho v\rangle}$ is zero. Using $\rho\,dw = \rho c_p\,dT + (1 - T\beta)\,dp$, we can write Eq. (37) as

$$\bar{H}_2 \simeq \phi A\rho_m c_{p,m}\overline{\text{Re}[u_1e^{i\omega t}]\text{Re}[T_1e^{i\omega t}]} + \phi A(1 - T_m\beta_m)\overline{\text{Re}[p_1e^{i\omega t}]\text{Re}[\langle u_1\rangle e^{i\omega t}]} - (1-\phi)AK_{\text{eff}}\frac{dT_m}{dx} \quad (38)$$

Recalling the definition of $\langle T\rangle_u$ from Eq. (24), we have

$$\tilde{H}_2 \simeq \phi A \rho_m c_{p,m} \overline{\mathrm{Re}[\langle u_1\rangle e^{i\omega t}]\mathrm{Re}[\langle T\rangle_{u,1} e^{i\omega t}]} + \phi A(1 - T_m\beta_m)\overline{\mathrm{Re}[p_1 e^{i\omega t}]\mathrm{Re}[\langle u_1\rangle e^{i\omega t}]} - (1 - \phi)AK_{\mathrm{eff}}\frac{dT_m}{dx} \tag{39}$$

This last step is subtle: the same kind of weighted average is needed for T in our energy flux equation as is used in the tabulated steady-state heat transfer coefficients for stacked screens.[15] The heat transfer tabulations of Kays and London[11] are based on measurements that used velocity-weighted average temperatures upstream and downstream of the screen test bed. This is extremely fortunate; otherwise, we would have little hope that either our harmonic calculation or time-step methods such as that of Gary et al.[2] would account for energy flux accurately, yet energy flux is one of the variables of greatest interest in high-effectiveness regenerators such as are used in Stirling cryocoolers.

Next, we substitute Eq. (29) for $\langle T\rangle_{u,1}$ into Eq. (39), and use Eq. (2) for the time averages. Solving the resulting equation for dT_m/dx, we obtain

$$\frac{dT_m}{dx} = \left\{\mathrm{Re}\left[\left(T_m\beta_m\frac{\varepsilon_s + \varepsilon_h(g_c + e^{2i\theta_p}g_v)}{1 + \varepsilon_s + \varepsilon_h(g_c + e^{2i\theta_T}g_v)} + 1 - T_m\beta_m\right)p_1\langle\tilde{u}cf l_1\rangle\right] - \frac{2\tilde{H}_2}{\phi A}\right\} \Bigg/ \left\{\frac{\rho_m c_{p,m}}{\omega}\mathrm{Im}\left[\frac{\varepsilon_s + \varepsilon_h(g_c - g_v)}{1 + \varepsilon_s + \varepsilon_h(g_c + e^{2i\theta_T}g_v)}\right]\langle u_1\rangle\langle\tilde{u}_1\rangle + 2K_{\mathrm{eff}}\frac{1 - \phi}{\phi}\right\} \tag{40}$$

This is the second of the three equations we seek; it is of the form of Eq. (5). Xiao[7] presented an equation of the same form, but it was greatly simplified because of his use of an amplitude-independent heat transfer coefficient.

D. Continuity Equation: $d\langle u_1\rangle/dx$

Finally, to obtain an expression for $d\langle u_1\rangle/dx$ of the form of Eq. (4), we use the continuity equation $\partial\rho/\partial t + \nabla\cdot\rho v = 0$. Performing the local spatial average, using expressions of the form of Eq. (1) for each variable, and keeping only first-order terms yields

$$i\omega\langle\rho_1\rangle + \frac{d(\rho_m\langle u_1\rangle)}{dx} = 0 \tag{41}$$

Oscillatory density $\langle\rho_1\rangle$ may be expressed in terms of p_1 and $\langle T_1\rangle$ using $d\rho = -\rho\beta\, dT + (\gamma/a^2)\, dp$, where γ is the ratio of isobaric to isochoric specific heats and a is the adiabatic sound speed. Writing $d\rho_m/dx = -\rho_m\beta\, dT_m/dx$ and solving the resulting equation for $d\langle u_1\rangle/dx$ yields

$$\frac{d\langle u_1\rangle}{dx} = i\omega\beta_m\langle T_1\rangle - \frac{i\omega\gamma_m}{\rho_m a_m^2}p_1 + \beta_m\frac{dT_m}{dx}\langle u_1\rangle \tag{42}$$

This equation is easy to understand for the case $\langle T_1\rangle = 0$: The two remaining terms on the RHS are caused by oscillating pressure and velocity. The pressure term is just the isothermal compressibility $\gamma/\rho_m a^2$ times $\partial p/\partial t$. The velocity term expresses continuity of mass flux $\rho_m\langle u_1\rangle$ in the presence of a temperature gradient and attendant density gradient.

If Eq. (42) contained $\langle T\rangle_{u,1}$ instead of $\langle T_1\rangle$, we could simply use Eq. (29) for $\langle T_1\rangle_u$ and our set of equations of the form of Eqs. (3–5) would be complete. Unfortunately, Eq. (42) contains $\langle T_1\rangle$. We have been unable to derive an alternative version of the continuity equation that uses $\langle T\rangle_{u,1}$ instead of $\langle T_1\rangle$, and we have found no data analogous to Kays and London's heat transfer data that can be used to predict $\langle T_1\rangle$. To our knowledge, previous work on stacked screen regenerators has not noted the distinction between these two temperature averages. In this report, we will simply proceed with the approximation that the two temperature averages are nearly equal, so that we will use

$$\frac{d\langle u_1\rangle}{dx} \simeq i\omega\beta_m\langle T\rangle_{u,1} - \frac{i\omega\gamma_m}{\rho_m a_m^2}p_1 + \beta_m\frac{dT_m}{dx}\langle u_1\rangle \tag{43}$$

with Eq. (29) for $\langle T\rangle_{u,1}$ as the last of the equations we seek, of the form of Eq. (4). The largest terms on the RHS of Eq. (43) are the second and third, which, respectively, represent the isothermal compressibility and thermal expansion of the gas as it moves along the temperature gradient. The first term on the right accounts for other, smaller effects caused by finite solid specific heat and imperfect thermal contact allowing oscillatory temperature.

Even though the largest terms on the RHS of Eq. (43) are correct, the first term cannot be ignored because some of the part of $d\langle u_1\rangle/dx$ that comes from $\langle T_1\rangle$ represents the mechanical power absorbed by the regenerator. To understand this, we consider the second-order work flow absorbed in length dx of the regenerator:

$$d\tilde{W}_2 = \phi A\, dx\frac{d\overline{(p_1\langle u_1\rangle)}}{dx} = \phi A\, dx\left(\overline{\langle u_1\rangle\frac{dp_1}{dx}} + \overline{p_1\frac{d\langle u_1\rangle}{dx}}\right) \tag{44}$$

The first term on the RHS represents power dissipated by viscosity, via the mechanisms accounted for in Eq. (12). The second term comes from thermal relaxation mechanisms accounted for in the first term of Eq. (43).

Equations similar in form to Eq. (43) were derived by Xiao[7] using an amplitude-independent heat transfer coefficient and by Huang and Lu[10] using amplitude-dependent heat transfer data of Tanaka et al.[14] Comparison of our effective heat transfer coefficient, embodied most clearly in Eq. (29), to the latter work is difficult for a number of reasons. First, our results show that the effective heat transfer coefficient depends on the magnitude of p_1 and on its phase, via the factor $e^{2i\theta_p}$ in Eq. (29); this effect has been ignored previously. Tanaka's results are based on measurements with a regenerator spanning a non-negligible temperature difference, over which thermophysical properties of the helium gas vary significantly, and in which ordinary axial conduction [our K_{eff} term in Eq. (39)] is significant. We believe the most appropriate way to compare our results to those of Tanaka is to set $p_1 = 0$ in Eqs. (29) and (39). With that approximation our effective Nusselt numbers are at most 20% higher than the experimental results of Tanaka's Fig. 9, always falling between his experimental results and his curve labeled London. We regard this as an acceptable agreement under the circumstances. Note that the complexity of Eqs. (29) and (39) suggests the difficulty of accurately separating multiple heat transfer effects from measurements of energy flow through regenerators in oscillating flow with significant temperature gradients; in particular, measurements of regenerator effectiveness made with negligible oscillating pressure may not be directly applicable to realistic Stirling operating conditions.

III. Comparison to Other Results

We incorporated this computation procedure into a program[13] already in use for thermodynamic calculations in oscillatory flow. The program includes an iterative algorithm and convenient I/O procedures for handling mixed boundary conditions. (It also includes modules for heat exchangers, ducts, pistons, etc., so that full Stirling systems can be modeled in

Table 2 Data for numerical computations

Variables	Frequency, Hz 55	350
Input		
Area	1.17 cm^2	10.4 cm^2
Length	5.0 cm	5.5 cm
Porosity	0.686	0.673
Hydraulic radius	13.9 μm	18.3 μm
Hot temperature	300 K	300 K
Cold temperature	80 K	110 K
Mean pressure	2.0 MPa	3.1 MPa
Hot volumetric velocity	3.65×10^{-4} m^3/s, 0 deg	5.13×10^{-3} m^3/s, 0 deg
Cold volumetric velocity	0.62×10^{-4} m^3/s, −52 deg	1.50×10^{-3} m^3/s, −92 deg
Results		
Energy flux (harmonic)	2.1 W	50 W
Energy flux (REGEN3)	2.0 W	46 W
Gross cooling power (harmonic)	5.4 W	36 W
Gross cooling power (REGEN3)	6.6 W	55 W

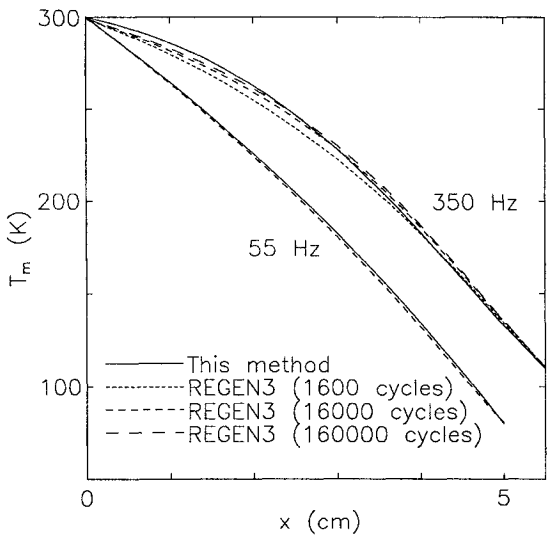

Fig. 2 Temperature profiles of 55- and 350-Hz regenerators, computed with the present method and with REGEN3.

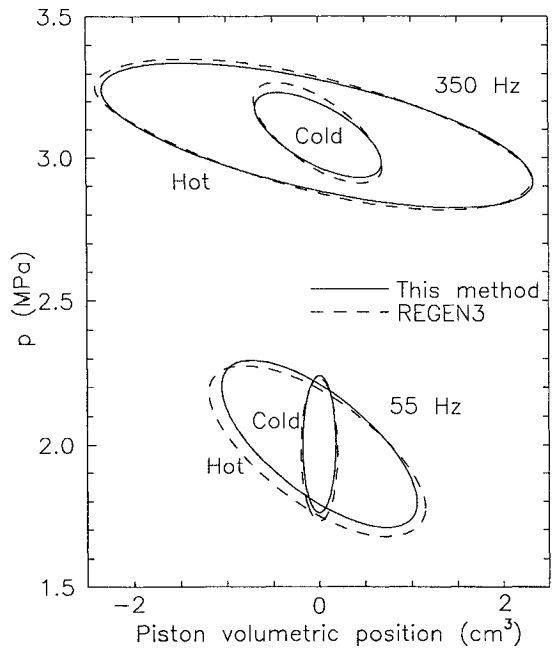

Fig. 3 Indicator diagrams at hot and cold ends of 55- and 350-Hz regenerators, computed with the present method and with REGEN3.

the harmonic approximation.) We tested our computation procedure by comparing the program's results with those of a time-step method that uses instantaneous friction factor and heat transfer: REGEN3 by Ref. 2. We checked results for a number of simplified cases, each designed to accentuate the effects of one physical process or part of the equations, such as verifying the implementation of the continuity equation without significant effects of viscous dissipation by computing for a short regenerator with oscillatory pressure but negligible oscillatory flow. We also compared results for a few realistic regenerators; two representative cases, at 55 and 350 Hz, are displayed here. Table 2 summarizes the geometry and other parameters for these two cases. (Volumetric velocity = $\phi A\langle u_1 \rangle$.) The 55-Hz case is a rather typical cryogenic regenerator, with $\delta_\kappa/r_h \sim 5$ at the cold end and 17 at the hot end, and with the viscous pressure drop about 20% of the oscillatory pressure. The 350-Hz case is atypical, with δ_κ/r_h only 1.7 at the cold end and 4 at the hot end, and with the viscous pressure drop amounting to 40% of the oscillatory pressure.

Computation of an accurate temperature profile is one of the most time-consuming aspects of time-step computation methods such as REGEN3, because the computation must proceed for as many thermodynamic cycles as are actually required for experimental hardware to reach thermal equilibrium. (REGEN3 speeds this process up significantly by allowing the user to declare a suitable guess for the midpoint temperature as well as the two end temperatures.) Figure 2 shows the temperature profiles computed for the two cases, using our harmonic method and REGEN3. The agreement is excellent. The results show that REGEN3's temperature profile may not be perfectly converged to steady state even after 160,000 thermodynamic cycles, particularly at the hot end of the regenerator where solid heat capacity, and, hence, equilibration time, are largest. (On a personal computer for which our harmonic computation required <1 s, the 160,000-cycle REGEN3 computation required 4 days.)

Figure 3 shows what are essentially pV indicator diagrams (or Lissajous figures) for the two cases. The vertical axis is pressure; the horizontal axis is the time integral of the volumetric velocity at the ends of the regenerator, essentially the volumetric position V of imaginary isothermal pistons located there. The volumetric velocities are given boundary conditions in these computations (see Table 2); the pressures as functions of time are computed results. Both the magnitude and phase of p calculated with our simple harmonic method are in good agreement with the REGEN3 results.

The area of each large (hot end) indicator diagram equals the power that must be supplied to the refrigerator. The two calculation methods give the same values of pV power within 20%. The harmonic approximation ensures that the pV curves are ellipses, whereas they are closed curves of more arbitrary

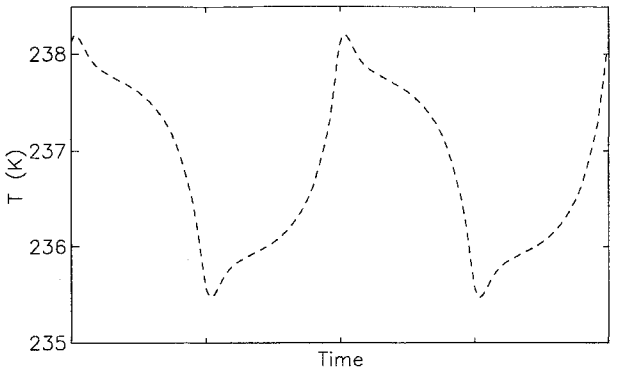

Fig. 4 Spatial average gas temperature as a function of time in the center of the 350-Hz regenerator, calculated with REGEN3. Two full cycles of the 350-Hz oscillation are shown.

shape in the REGEN3 analysis. In the general case with V and p both written as Fourier series

$$V = \sum_{n=1}^{\infty} \mathrm{Re}[V_n e^{in\omega t}], \qquad p = \sum_{n=1}^{\infty} \mathrm{Re}[p_n e^{in\omega t}] \tag{45}$$

the mechanical power is $\overline{pV} = \frac{1}{2} \Sigma_n \mathrm{Re}[in\omega p_n \tilde{V}_n]$. There are no cross terms. Hence, in comparison with REGEN3 results, where $V_n = 0$ for $n \neq 1$ at the ends of the regenerator, the harmonic method's neglect of p_n for $n \geq 2$ has no effect on work.

Returning to Table 2, we find that the energy fluxes through the regenerator calculated by the two methods agree to 10%. This good agreement might at first seem remarkable, given the fact that REGEN3 calculations of oscillatory temperature (see Fig. 4) show that the actual temperature is far from sinusoidal. However, an argument similar to that previously for pV work shows that harmonics have little effect on the time-averaged energy flux. The hydrodynamic part of the energy flux density is given by $\rho c_p T u$ for an ideal gas. Assuming constant c_p as appropriate for an ideal gas, with the realization that $\overline{\rho u} = 0$ because there is no time-averaged mass flux through the regenerator, and expanding T and u in Fourier series as we did earlier for p and V yields $\frac{1}{2} c_p \Sigma_n \mathrm{Re}[(\rho u)_n \tilde{T}_n]$. Again, there are no cross terms. In general, if harmonic content of both T and u is of order ε, the harmonic contribution to energy flux is of order ε^2, so the harmonic method can be expected to give acceptably accurate energy results even for substantial harmonic content. In the case of REGEN3, $u_n = 0$ for $n \neq 1$ at the ends, so we expect that u_n would be small for $n \neq 1$ throughout the regenerator. Hence, the hydrodynamic part of the energy flux is very well approximated by only the fundamental components of T and u.

Finally, returning to Table 2, we examine the results for gross cooling power, the difference between pV power extracted by the cold piston and energy flux through the regenerator. This is the quantity of greatest interest; it is also the most difficult to compute, as it is the difference between two numbers of similar magnitude, each of which is the time-averaged product of oscillatory quantities. The gross cooling powers agree to 20% for the conventional regenerator and 40% for the 350-Hz regenerator. The greater disagreement in the latter case may be because of our use of REGEN3 in a regime of large viscous pressure drop, for which it was never intended.

Appendix A: Fits to Kays and London Plots

In this appendix we present our simple fits to the friction factor and heat transfer coefficient plots in Kays and London.[11]

The solid curves in the upper half of Fig. A1 are taken from Kays and London's Fig. 7-9, showing friction factor vs Reynolds number for three values of porosity. To generate a fit of the form of Eq. (9), we choose to set $c_n(\phi) \equiv 0$ for $n \geq 3$, and to let c_1 and c_2 be quadratic functions of porosity that fit Kays and London data well at $Re = 8$ and 40. This leads to

$$c_1(\phi) = 1268 - 3545\phi + 2544\phi^2 \tag{A1}$$

$$c_2(\phi) = -2.82 + 10.7\phi - 8.6\phi^2 \tag{A2}$$

The values of f obtained from Eqs. (9), (A1), and (A2) are shown as dashed lines in Fig. A1. The agreement with the Kays and London curves, at the 13% level below $R = 1000$, is adequate for this work.

The solid curves in the lower half of Fig. A1 are taken from Kays and London's Fig. 7-8, and show heat transfer coefficient as a function of Reynolds number. The curves are nearly straight lines with slope $-2/5$ on this log–log plot, implying $h \sim Re^{3/5}$. But this dependence would imply that $h \to 0$ as $Re \to 0$, whereas we know that h must approach something of the order of K/r_h at low Reynolds numbers. To accommodate a plausible low Reynolds number limit in a mathematically simple way, while keeping the 3/5 power law at high Reynolds numbers, we choose to write

$$h(Re) = \frac{b(\phi)\sigma^{1/3}}{4} \frac{K}{r_h} (1 + Re^{3/5}) \tag{A3}$$

The details of this low-Reynolds cutoff are unimportant for energy flux and the resulting expression for dT_m/dx, because significant enthalpy is carried only at high velocities and, hence, at high Reynolds numbers. However, thermal relaxation dissipates power, which we calculate via the continuity equation and the resulting Eq. (43) for $d\langle u_1 \rangle/dx$. Some of that thermal relaxation occurs at and near zero velocity, especially to the extent that p_1 is in phase with $\langle u_1 \rangle$, as it is in Stirling machines. A better low-Reynolds version of Eq. (A3), based on laboratory measurements of h at very low Reynolds numbers, would probably improve the accuracy of $d\langle u_1 \rangle/dx$ and work computations in stacked-screen regenerators, both in the simple harmonic method and in other methods.

As with the friction factor data, we choose to write b as a quadratic function of ϕ, fitting the Kays and London plots well at $Re = 20$. The result is

$$b(\phi) = 3.81 - 11.29\phi + 9.47\phi^2 \tag{A4}$$

The dashed lines in the lower half of Fig. A1 are plots of Eq. (A3) using Eq. (A4). The agreement with the Kays and London curves, <10% for $10 < Re < 10^3$, is adequate for this work.

Appendix B: Calculation of g_c and g_v

It would be very slow to re-evaluate $g_c(Re_1)$ and $g_v(Re_1)$ using Eqs. (30) and (31) each time they are needed during full numerical integration of a regenerator, so we have developed simpler approximations for these functions that can be computed rapidly.

At low Reynolds numbers, the integrands in Eqs. (30) and (31) can be expanded as power series in the small quantity $Re_1^{3/5} \cos^{3/5} z$, and the integrations performed term by term. This yields

$$g_{c,\mathrm{low}} \to 1 - \frac{\Gamma(0.8)}{\sqrt{\pi}\Gamma(1.3)} Re_1^{3/5} + \frac{\Gamma(1.1)}{\sqrt{\pi}\Gamma(1.6)} Re_1^{6/5} - \frac{\Gamma(1.4)}{\sqrt{\pi}\Gamma(1.9)} Re_1^{9/5} + \cdots \simeq 1 - 0.73188 Re_1^{3/5} + 0.59993 Re_1^{6/5} - 0.52048 Re_1^{9/5} \tag{B1}$$

where Γ is the ordinary gamma function, and similarly

$$g_{v,\mathrm{low}} \simeq 0.16890 Re_1^{3/5} - 0.22604 Re_1^{6/5} + 0.24654 Re_1^{9/5} - 0.25379 Re_1^{12/5} + 0.25465 Re_1^{3} \tag{B2}$$

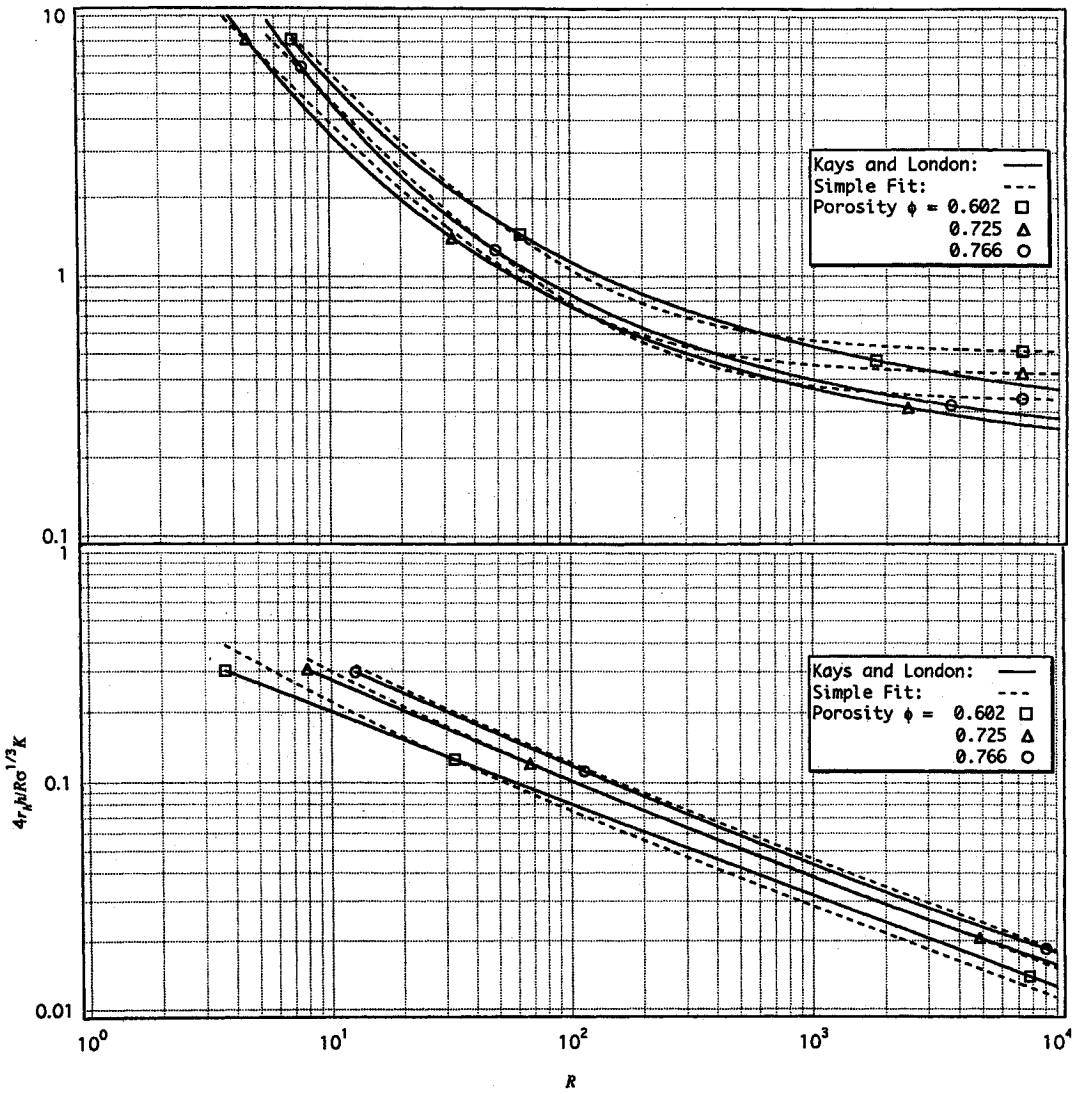

Fig. A1 Friction factor and heat transfer coefficient vs Reynolds number from Ref. 11, and our simple fits to them.

Numerical integrations of Eqs. (30) and (31) were used to confirm these low Reynolds number expressions and to compute values for higher Reynolds numbers. With simple functional fits we finally arrived at the following expressions:

$$g_c = f_{c,\text{hi}} g_{c,\text{hi}} + f_{c,\text{low}} g_{c,\text{low}} \tag{B3}$$

where

$$f_{c,\text{hi}} = 1/(1 + 2.9Re_1^{-3}), \qquad f_{c,\text{low}} = 1/(1 + 0.33Re_1^{3})$$
$$g_{c,\text{hi}} = 1.2915Re_1^{-0.55338} \tag{B4}$$

and $g_{c,\text{low}}$ is given by Eq. (B1); and

$$g_v = f_{v,\text{hi}} g_{v,\text{hi}} + (1 - f_{v,\text{low}} - f_{v,\text{hi}}) g_{v,\text{mid}} + f_{v,\text{low}} g_{v,\text{low}} \tag{B5}$$

where

$$f_{v,\text{hi}} = 1/(1 + 715Re_1^{-2}), \qquad f_{v,\text{low}} = 1/(1 + 100Re_1^{5})$$
$$g_{v,\text{hi}} = 0.405Re_1^{-0.53} \tag{B6}$$
$$g_{v,\text{mid}} = 0.0679 - 0.00685[\ell n(Re_1) - 0.884]^2$$

and $g_{v,\text{low}}$ is given by Eq. (B2). Figure B1 shows our numerical integrations of Eqs. (30) and (31) and our simpler expressions given in Eqs. (B1–B6).

Appendix C: Details of $\langle T \rangle_{u,1}$ Derivation

In this appendix we outline the steps required to derive Eq. (29) from Eq. (25) in the main text. We must multiply Eq. (25) by $e^{-i\omega t}/\pi$ and integrate from 0 to 2π with respect to ωt to select the fundamental, complex Fourier component. There are four terms (two on the LHS and two on the RHS).

The first term is

$$\frac{(1 + \varepsilon_s)}{\pi} \int_0^{2\pi} e^{-i\omega t} \frac{\partial \langle T \rangle_u}{\partial t} \, \mathrm{d}(\omega t) \tag{C1}$$

Substituting an expression of the form of Eq. (1) for $\langle T \rangle_u$, the integration easily and immediately yields

$$i\omega(1 + \varepsilon_s)\langle T \rangle_{u,1} \tag{C2}$$

The second term is

$$\frac{\rho_m c_{p,m} r_h}{\pi} \int_0^{2\pi} e^{-i\omega t} \frac{\partial}{\partial t} \left[\frac{1}{h(Re)} \frac{\partial \langle T \rangle_u}{\partial t} \right] \mathrm{d}(\omega t) \tag{C3}$$

Integrating by parts to eliminate one time derivative, we obtain

$$\frac{i\omega \rho_m c_{p,m} r_h}{\pi} \int_0^{2\pi} e^{-i\omega t} \frac{1}{h(Re)} \frac{\partial \langle T \rangle_u}{\partial t} \, \mathrm{d}(\omega t) \tag{C4}$$

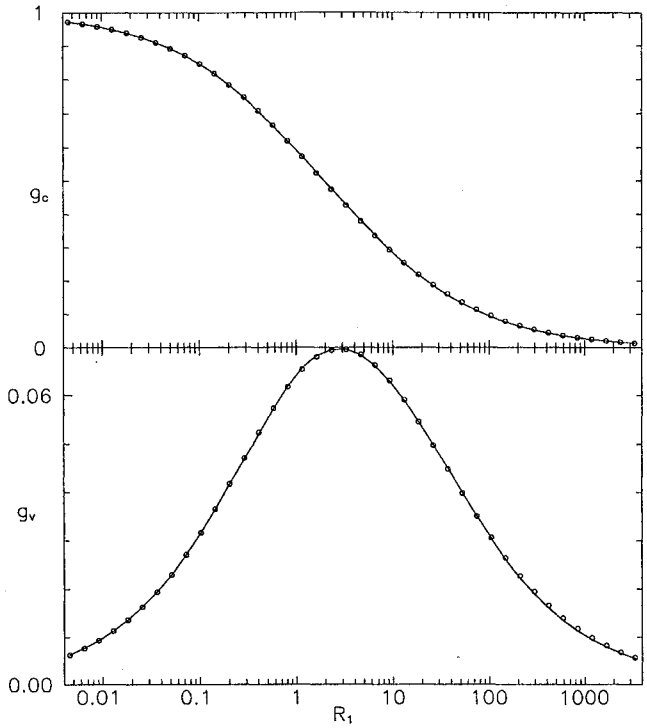

Fig. B1 Functions g_c and g_v vs Reynolds number. The points are the results of numerical integrations of the equations in the main text. The solid curves were evaluated using the simpler expressions in Appendix B.

We next substitute Eq. (28) for h and use expressions of the form of Eq. (1) for $\langle T\rangle_u$ and $\langle u\rangle$. With α_T and α_u defined by $\langle T\rangle_{u,1} = |\langle T\rangle_{u,1}|e^{i\alpha_T}$ and $\langle u_1\rangle = |\langle u_1\rangle|e^{i\alpha_u}$, we can express Eq. (C4) as

$$-\frac{\omega\varepsilon_h}{\pi}\int_0^{2\pi}\frac{e^{-iy}|\langle T\rangle_{u,1}|\sin(y+\alpha_T)}{1+Re_1^{3/5}|\cos(y+\alpha_u)|^{3/5}}\,dy \tag{C5}$$

where

$$\varepsilon_h = 8ir_h^2/b(\phi)\sigma^{1/3}\delta_\kappa^2 \tag{C6}$$

Let $z = y + \alpha_u$. The integrand has period π, so we can begin the integration at any angle, end at that angle $+\pi$, and double the result. We choose the integration limits so that we can eliminate the absolute value in the denominator:

$$-\frac{2\omega\varepsilon_h\langle T\rangle_{u,1}}{\pi}\int_{-\pi/2}^{\pi/2}\frac{e^{-i(z-\theta_T)}\sin(z-\theta_T)}{1+Re_1^{3/5}\cos^{3/5}z}\,dz \tag{C7}$$

where $\theta_T = \alpha_u - \alpha_T$ is the phase angle by which temperature lags velocity. The denominator is an even function of z. Because the integration limits are even, any pieces of the numerator that are odd in z contribute nothing. Using standard trigonometric identities in the numerator, we obtain

$$\frac{4i\omega\varepsilon_h\langle T\rangle_{u,1}}{\pi}\int_0^{\pi/2}\frac{e^{i\theta_T}(\sin^2 z\cos\theta_T - i\cos^2 z\sin\theta_T)}{1+Re_1^{3/5}\cos^{3/5}z}\,dz$$

which can be rewritten

$$i\omega\varepsilon_h(g_c + e^{2i\theta_T}g_v)\langle T\rangle_{u,1} \tag{C8}$$

where g_c and g_v are given by Eqs. (30) and (31).

The third term is

$$\frac{\varepsilon_s}{\pi}\int_0^{2\pi}\left(\frac{T_m\beta_m}{\rho_m c_{p,m}}\frac{\partial p}{\partial t} - \frac{dT_m}{dx}\langle u\rangle\right)e^{-i\omega t}\,d(\omega t) \tag{C9}$$

Substituting expressions of the form of Eq. (1) for p and $\langle u\rangle$ and performing the integration easily yields

$$\varepsilon_s\left(\frac{T_m\beta_m}{\rho_m c_{p,m}}i\omega p_1 - \frac{dT_m}{dx}\langle u_1\rangle\right) \tag{C10}$$

The fourth term is

$$\frac{\rho_m c_{p,m} r_h}{\pi}\int_0^{2\pi}e^{-i\omega t}\frac{\partial}{\partial t}\left[\frac{1}{h(Re)}\left(\frac{T_m\beta_m}{\rho_m c_{p,m}}\frac{\partial p}{\partial t} - \frac{dT_m}{dx}\langle u\rangle\right)\right]d(\omega t) \tag{C11}$$

As we did earlier with the second term, we integrate by parts

$$\frac{\varepsilon_h}{\pi}\int_0^{2\pi}\frac{e^{-iy}\,dy}{1+Re_1^{3/5}|\cos(y+\alpha_u)|^{3/5}}\left[-\omega\frac{T_m\beta_m}{\rho_m c_{p,m}} \times |p_1|\sin(y+\alpha_p) - \frac{dT_m}{dx}|\langle u_1\rangle|\cos(y+\alpha_u)\right] \tag{C12}$$

and choose the limits of integration to eliminate the absolute value:

$$\frac{2\varepsilon_h}{\pi}\int_{-\pi/2}^{\pi/2}\frac{dz}{1+Re_1^{3/5}\cos^{3/5}z}\left[-\omega\frac{T_m\beta_m}{\rho_m c_{p,m}}p_1 e^{-i(z-\theta_p)} \times \sin(z-\theta_p) - \frac{dT_m}{dx}\langle u_1\rangle e^{-iz}\cos z\right] \tag{C13}$$

where $\theta_p = \alpha_u - \alpha_p$. The part of the integrand involving p_1 is similar to the second term [Eq. (C8)]. The part of the integrand involving $\langle u_1\rangle$ is easy. The result is

$$\varepsilon_h\left[i\omega\frac{T_m\beta_m}{\rho_m c_{p,m}}(g_c + e^{2i\theta_p}g_v)p_1 - \frac{dT_m}{dx}(g_c - g_v)\langle u_1\rangle\right] \tag{C14}$$

where $\theta_p = \alpha_u - \alpha_p$ is the phase angle by which pressure lags velocity.

Combining Eqs. (C2), (C8), (C10), and (C14), we obtain Eq. (29).

Appendix D: Computation Details

In this appendix, we gather for convenience the final results from the previous sections, and summarize the method of computation.

We begin at one end of the regenerator, with $\bar{H}_2$ given and with given initial values of (real) T_m, (complex) p_1, and (complex) $\langle u_1\rangle$. We then generate $T_m(x)$, $p_1(x)$, and $\langle u_1(x)\rangle$ by numerical integration along x using

$$\frac{dp_1}{dx} = -i\omega\rho_m\left[1 + \frac{(1-\phi)^2}{2(2\phi-1)}\right]\langle u_1\rangle - \frac{\mu_m}{r_h^2}\left[\frac{c_1(\phi)}{8} + \frac{c_2(\phi)Re_1}{3\pi}\right]\langle u_1\rangle \tag{D1}$$

$$\frac{d\langle u_1\rangle}{dx} = -\frac{i\omega\gamma_m}{\rho_m a_m^2}p_1 + \beta_m\frac{dT_m}{dx}\langle u_1\rangle + i\omega\beta_m\left[\frac{T_m\beta_m}{\rho_m c_{p,m}}\frac{\varepsilon_s + (g_c + e^{2i\theta_p}g_v)\varepsilon_h}{1+\varepsilon_s + (g_c + e^{2i\theta_T}g_v)\varepsilon_h}p_1 - \frac{1}{i\omega}\frac{dT_m}{dx}\frac{\varepsilon_s + (g_c - g_v)\varepsilon_h}{1+\varepsilon_s + (g_c + e^{2i\theta_T}g_v)\varepsilon_h}\langle u_1\rangle\right] \tag{D2}$$

$$\frac{dT_m}{dx} = \left\{ \mathrm{Re}\left[\left(T_m\beta_m \frac{\varepsilon_s + \varepsilon_h(g_c + e^{2i\theta_p}g_v)}{1 + \varepsilon_s + \varepsilon_h(g_c + e^{2i\theta_T}g_v)} + 1 - T_m\beta_m \right) p_1\langle\tilde{u}_1\rangle \right] - \frac{2\bar{H}_2}{\phi A} \right\} \Bigg/ \left\{ \frac{\rho_m c_{p,m}}{\omega} \times \mathrm{Im}\left[\frac{\varepsilon_s + \varepsilon_h(g_c - g_v)}{1 + \varepsilon_s + \varepsilon_h(g_c + e^{2i\theta_T}g_v)} \right] \langle u_1\rangle\langle\tilde{u}_1\rangle + 2K_{\mathrm{eff}} \frac{1-\phi}{\phi} \right\} \tag{D3}$$

using

$$c_1(\phi) = 1268 - 3545\phi + 2544\phi^2$$
$$c_2(\phi) = -2.82 + 10.7\phi - 8.6\phi^2 \tag{D4}$$

$$b(\phi) = 3.81 - 11.29\phi + 9.47\phi^2 \tag{D5}$$

$$Re_1 = 4|\langle u_1\rangle| r_h\rho_m/\mu_m \tag{D6}$$

$$\varepsilon_s = \phi\rho_m c_{p,m}/(1-\phi)\rho_{s,m}c_{s,m}, \qquad \varepsilon_h = 8ir_h^2/b(\phi)\sigma^{1/3}\delta_\kappa^2 \tag{D7}$$

$$\delta_\kappa^2 = 2K_m/\omega\rho_m c_{p,m} \tag{D8}$$

$$\theta_p = \mathrm{phase}(\langle u_1\rangle) - \mathrm{phase}(p_1)$$
$$\theta_T = \mathrm{phase}(\langle u_1\rangle) - \mathrm{phase}(\langle T\rangle_{u,1}) \tag{D9}$$

$$g_c = \frac{2}{\pi}\int_0^{\pi/2} \frac{dz}{1 + Re_1^{3/5}\cos^{3/5}(z)}$$
$$g_v = -\frac{2}{\pi}\int_0^{\pi/2} \frac{\cos(2z)\,dz}{1 + Re_1^{3/5}\cos^{3/5}(z)} \tag{D10}$$

This procedure generates (among other things) the values of T_m, p_1, and $\langle u_1\rangle$ at the final end of the regenerator. If all of the initial values are not known, but instead some boundary conditions are specified at the final end, a shooting method is used to adjust the unknown initial values until the known final values are reached.

Acknowledgments

This work has been supported by the TTI program of the U.S. Department of Energy, and by the Tektronix Corporation. We are most grateful to Ray Radebaugh and Charles Jin for help with REGEN3. We thank Terry Hendricks for pointing out the connection to the extensive literature on oscillatory flow in isotropic porous media.

References

[1]Organ, A. J., *Thermodynamics and Gas Dynamics of the Stirling Cycle Machine*, Cambridge Univ. Press, Cambridge, England, UK, 1992.

[2]Gary, J., O'Gallagher, A., and Radebaugh, R., "A Numerical Model for Regenerator Performance," National Institute of Standards and Technology, Boulder, CO, 1994; also *REGEN 3.1 Users Guide*.

[3]Gedeon, D., "A Globally Implicit Stirling Cycle Simulation," *Proceedings of the 21st International Energy Conversion Engineering Conference*, American Chemical Society, Washington, DC, 1986, p. 550.

[4]Bauwens, L., "Near-Isothermal Regenerator: A Perturbation Analysis," *Journal of Thermophysics and Heat Transfer*, Vol. 9, No. 4, 1995, pp. 749–756.

[5]Urieli, I., and Berchowitz, D. M., *Stirling Cycle Engine Analysis*, Adam Hilger, Bristol, England, UK, 1984.

[6]Organ, A. J., "Steady-Flow C_f-N_{Re} Correlation for the Wire Gauze Regenerator Inferred from Linear Wave Analysis; Flow in the Stirling Regenerator Characterized in Terms of Complex Admittance, Part 1 and Part 2," *Proceedings — Institution of Mechanical Engineers*, Vol. 207, Nos. C1, C2, 1993, pp. 53–60, 117–139.

[7]Xiao, J. H., "Thermoacoustic Theory for Cyclic Flow Regenerators. Part I: Fundamentals," *Cryogenics*, Vol. 32, No. 10, 1992, pp. 895–901.

[8]Xiao, J. H., "Thermoacoustic Theory for Regenerative Cryocoolers," *Proceedings of the 7th International Cryocoolers Conference* (Santa Fe, NM), U.S. Air Force Rept. PL-CP-93-1001, Nov. 1993.

[9]Huang, B. J., and Lu, C. W., "Dynamic Response of Regenerator in Cyclic Flow System," *Cryogenics*, Vol. 33, No. 11, 1993, pp. 1046–1052.

[10]Huang, B. J., and Lu, C. W., "Linear Network Analysis of Regenerator in a Cyclic-Flow System," *Cryogenics*, Vol. 35, No. 3, 1995, pp. 203–207.

[11]Kays, W. M., and London, A. L., *Compact Heat Exchangers*, McGraw–Hill, New York, 1964.

[12]Mitchell, M. P., Yaron, R., Shokralla, S., Yuan, J., Bradley, P. E., and Radebaugh, R., "Etched Foil Regenerator," *Advances in Cryogenic Engineering* (to be published).

[13]Ward, W. C., and Swift, G. W., "Design Environment for Low Amplitude Thermoacoustic Engines," *Journal of the Acoustical Society of America*, Vol. 95, No. 6, 1994, pp. 3671–3672.

[14]Tanaka, M., Yamashita, I., and Chisaka, F., "Flow and Heat Transfer Characteristics of the Stirling Engine Regenerator in an Oscillating Flow," *JSME International Journal, Series II*, Vol. 33, No. 2, 1990, pp. 283–289.

[15]Radebaugh, R., private communication, Boulder, CO, 1994.